agriculture

MDPI

Article

An Ultrasonic Ridge-Tracking Method Based on Limiter Sliding Window Filter and Fuzzy Pure Pursuit Control for Ridge Transplanter

Wei Liu [1], Jinhao Zhou [1], Yutong Liu [1], Tengfei Zhang [1], Meng Yan [1], Ji Chen [2], Chunjian Zhou [2], Jianping Hu [1] and Xinxin Chen [1,*]

[1] School of Agricultural Engineering, Jiangsu University, Zhenjiang 212013, China; mario_liu@ujs.edu.cn (W.L.); 2112316042@stmail.ujs.edu.cn (J.Z.); 2222016041@stmail.ujs.edu.cn (Y.L.); 2112016001@stmail.ujs.edu.cn (T.Z.); 2212016059@stmail.ujs.edu.cn (M.Y.); hujp@ujs.edu.cn (J.H.)

[2] Shanghai Agricultural Machinery Research Institute, Shanghai 201106, China; shnjscj@163.com (J.C.); shnjszcj@163.com (C.Z.)

* Correspondence: xxchen@ujs.edu.cn; Tel.: +86-195-9996-2668

Abstract: There are various types of fruits and vegetables that need to be planted on ridges. In order to allow for seedlings with a certain row space and seedling space, the ridge transplanter should be able to track along the ridge. Therefore, an ultrasonic ridge-tracking method and system were developed to let the ridge transplanter track the ridge accurately. The ultrasonic ridge-tracking method mainly contains a limiter sliding window filtering algorithm and a fuzzy look-ahead distance decision model. The limiter sliding window filtering algorithm was proposed to filter the abnormal measuring results to avoid disoperation of the steering mechanism. Moreover, the fuzzy look-ahead distance decision model was proposed to determine the optimal look-ahead distance in order to obtain a desirable tracking performance. Additionally, a comparison experiment of the proposed ultrasonic ridge-tracking method and the universal pure pursuit method was conducted. The experimental results show that the greatest mean absolute errors of the lateral deviations of the ultrasonic ridge-tracking method and universal pure pursuit were 10.56 mm and 13.11 mm. The greatest maximum absolute errors of the lateral deviations of the ultrasonic ridge-tracking method and universal pure pursuit were 18.87 mm and 23.23 mm. In addition, the greatest root mean square error of the lateral deviation of the ultrasonic ridge-tracking method and the universal pure pursuit method were 13.52 mm and 15.66 mm. According to the ridge-tracking performance of the proposed ultrasonic ridge-tracking method, it can be used in practical transplanting conditions. Moreover, in other fields, robots or intelligent machinery can also apply the proposed ultrasonic ridge-tracking method to track objects similar to ridges.

Keywords: ultrasonic measuring; path tracking; ridge; transplanter; filter; pure pursuit

Citation: Liu, W.; Zhou, J.; Liu, Y.; Zhang, T.; Yan, M.; Chen, J.; Zhou, C.; Hu, J.; Chen, X. An Ultrasonic Ridge-Tracking Method Based on Limiter Sliding Window Filter and Fuzzy Pure Pursuit Control for Ridge Transplanter. *Agriculture* **2024**, *14*, 1713. https://doi.org/10.3390/agriculture14101713

Academic Editor: Mustafa Ucgul

Received: 30 August 2024
Revised: 25 September 2024
Accepted: 27 September 2024
Published: 29 September 2024

1. Introduction

A variety of fruits and vegetables, such as the strawberry, tomato, cucumber, and so on, need to be planted on ridges. The fruit and vegetable seedlings are usually transplanted onto ridges with a certain row spacing and line spacing by ridge transplanters. Thus, the ridge transplanter needs to track along the ridge, so as to keep accurate and stable row spaces and avoid the seedlings planting out of the ridge [1].

However, because in most cases the ridgers are driven manually, the curvatures of ridges may not be straight. Hence, the ridge-tracking performance of the ridge transplanter is crucial to the transplanting quality. Moreover, due to the wheels of the transplanter being in the furrow, the yaw of the transplanter was caused by the forces of the uneven ground on the wheels. Hence, according to the above two reasons, the heading angle of the transplanter should be controlled in real time [2]. Up to now, the steering of ridge

transplanter has been mainly controlled by the operator [3]. Therefore, in order to reduce the labor costs and improve the transplanting quality, the autonomous ridge-tracking method of the ridge transplanter needs to be developed.

Essentially, ridge tracking is a special type of path tracking with position constraints between the agricultural machinery and the ridge. There are three path-tracking methods commonly used in agricultural machinery, namely the kinematic method [4], dynamic method [5], and model-free method [6]. The kinematic method is easy to implement and is thus widely used [7]. The kinematic methods mainly consist of the pure pursuit tracking (PPT) method, the linear quadratic regulator (LQR) method, and the model predictive control (MPC) method. The PPT method selects a series of points in the reference path as look-ahead points, and then the agricultural machinery tracks the preset path by approaching the look-ahead points in order [8,9].

The LQR method and MPC method conduct enormous iterative computations to predict the future behaviors of the agricultural machinery. The optimal control inputs are selected according to the computation results [10]. A linear time-varying MPC algorithm was developed for path tracking based on the autonomous front-wheel steering system [11], and a conventional MPC algorithm was also improved based on the recursive least squares method with an adaptive forgetting factor [12]. Due to massive calculations, the LQR and MPC methods are usually time-consuming and model-dependent [13], so they may not be ideal for real-time ridge-tracking situations. If the steering of the ridge transplanter cannot be controlled in time, then the ridge will be damaged by the ridge transplanter.

The kinematic methods are easily affected by disturbances and thus lack robustness [7]. Therefore, some researchers developed path-tracking algorithms based on the dynamic models of agricultural machinery [14]. Among the dynamic methods, the sliding mode control (SMC) algorithm stands out as the most classical one. Raghavendra et al. proposed an intelligent SMC method to improve the path-tracking performance of the autonomous vehicle under the condition of parameter uncertainties. This method employed fractional order sliding manifolds, optimized sliding coefficients, and used fuzzy adaptive switching gain to enhance the tracking performance [15]. Although the SMC method can effectively eliminate environmental noise and has strong robustness, when system states slide along the slide mode surface, the machinery system may be chattered, which could affect the tracking performance of the agricultural machinery [16].

Because some parameters, such as the friction coefficient between the tire and ground, the vehicle load distribution, and so on, are difficult to measure, building a precise kinematic or dynamic model of agricultural machinery is still a challenge [17]. Therefore, more and more studies are focused on model-free path-tracking methods to overcome the time-varying and nonlinear characteristics of the agricultural machinery.

The PID control algorithm is the most widely applied among the model-free path-tracking methods. Zhang et al. applied a comprehensive performance index to optimize the PID controller for the agricultural wheeled vehicle whose kinematic model was the Ackerman model. The results showed that the overshoot and regulation time of the optimized control system were 10.03% and 3.95 s [18]. The PID control algorithm is easy to implement in practice. However, the typical PID controller has certain coefficients, which are not adaptable to the agricultural environment with time-varying parameters and external disturbances [19].

So as to overcome the above limitations, some nonlinear path-tracking algorithms that combine the PID and coefficient-determining algorithms were proposed. Fuzzy inference can determine the optimal parameters according to variable environmental conditions [20]. The steering angle of agricultural machinery was regulated in real time by a parameter-variable PID-controlling algorithm whose proportional, integral, and differential coefficients were determined by fuzzy rules [21]. The experimental results showed that the maximal lateral error and heading error of the developed path-tracking system were 4.39 cm and 2.13°.

Although some studies have been conducted to let the agricultural machinery track a reference path on a flat field ground [22], few studies have considered how to navigate machinery along a ridge with a variable curvature. Some positioning sensors, like GPS, cannot detect the position of the ridge, while machine vision or LiDAR would be affected by hard light. In order to overcome the mentioned sensing problems, the developed ridge-tracking method in this research used ultrasonic sensors to monitor the relative position between the ridge and the transplanter.

Hence, the goal of this study was to develop an ultrasonic ridge-tracking (URT) method for ridge transplanters to track along the ridge accurately. The proposed URT method mainly consists of two sections. One is a limiter sliding window filtering algorithm and the other is a fuzzy look-ahead distance decision method. In detail, the limiter sliding window (LSW) filtering algorithm was used to reduce the influence of the abnormal measuring results caused by ridge damage. Using the developed fuzzy look-ahead distance decision model, the optimal look-ahead distance can be determined and adjusted in real time based on the current lateral deviation and traveling velocity. Additionally, the field experiments were conducted to compare the performance of the proposed URT method and the universal pure pursuit (UPP) method.

2. Materials and Methods

2.1. Overall Research and Development Approach

In this research, the development of the ridge-tracking system used the reverse engineering approach [23]. The procedures of the development approach are displayed in Figure 1. First, the functions of the ridge-tracking system were analyzed, and then the kinematic model of the transplanter was developed. Moreover, in order to improve the tracking accuracy, the key sub-methods, i.e., the LSW filtering algorithm and fuzzy look-ahead distance decision model, were proposed. Finally, the ridge-tracking performance of the developed ultrasonic ridge-tracking method was validated in a greenhouse. The developed ultrasonic ridge-tracking method used the above sequence.

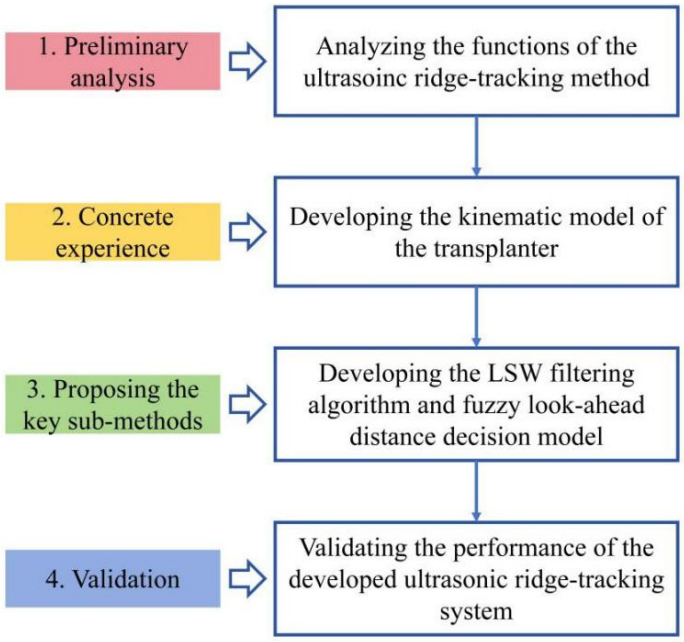

Figure 1. Flowchart of the research and development sequence of the ultrasonic ridge-tracking method.

2.2. Structure and Working Principle of the Transplanter Chassis

The proposed ultrasonic ridge-tracking method was applied to the developed transplanter chassis. The structure of the developed transplanter chassis is illustrated in Figure 2. The chassis contained two sections. One was the steering mechanism and the other was

the driving mechanism. The steering mechanism consisted of a steering motor, a steering reducer, a rack and gear mechanism, a slide guide rail, two sliders, and two steering rods.

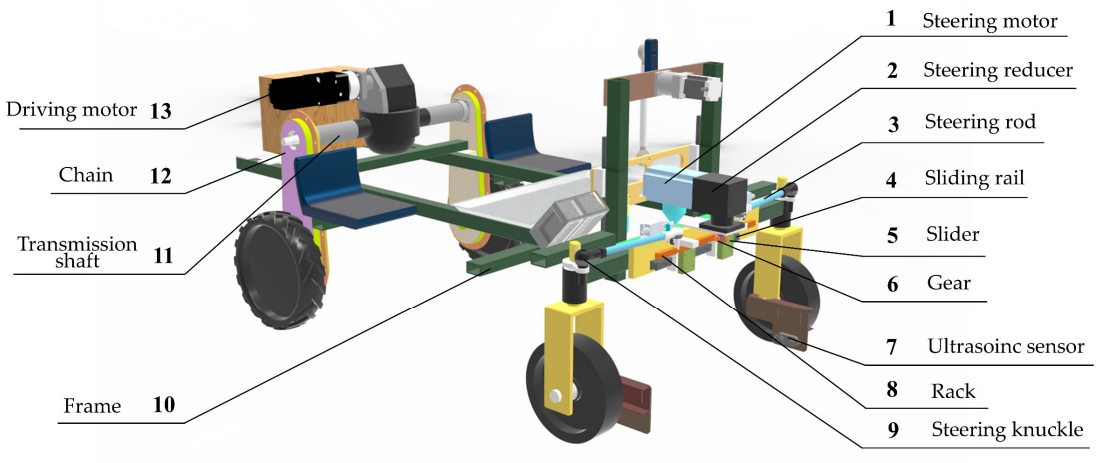

Figure 2. Structure of the developed transplanter chassis.

The working principle of the steering mechanism can be explained as follows. The output shaft of the steering motor connected to the input shaft of the reducer, and the output shaft of the reducer was fixed to a gear that was used to drive the rack for transverse motions. Two sliders mounted on the sliding rail were used to support the rack. Moreover, the steering rod connected to the slider and the steering knuckle of front wheel. Therefore, according to the theory of the aforementioned steering mechanism, the steering angle of the front wheel was controlled by the rotating angle of the steering motor.

As for the driving mechanism, its working principle can be explained as follows. The driving mechanism was composed of a driving motor, a reducer, two transmission shafts, and two chain systems. The driving motor connected to the reducer to expand the driving torque. The reducer had two symmetric output shafts, which connected to the left and right transmission shaft, respectively. The transmission shafts connected to the reducer and the sprocket wheel, which used chains to drive the rear wheels. The structural parameters of the chassis of the ridge transplanter are shown in Table 1.

Table 1. Structural parameters of the chassis of the ridge transplanter.

Structural Parameters	Value
Length (mm)	1700
Width (mm)	1300
Distance between wheels (mm)	800
Wheel base (mm)	1230
Maximum steering angle (°)	30
Suitable height of ridge (mm)	250–360

2.3. Developed Ultrasonic Ridge-Tracking System

The developed ultrasonic ridge-tracking system contained two ultrasonic sensors (DYP-A02YY-V2.0, Shenzhen Dianyingpu Technology Ltd., Shenzhen, China), a programmable logical controller PLC (XD3-32T-C, Wuxi XINJIE company limited by shares, Wuxi, China), an embedded signal acquisition system (ESAS) based on a micro control unit, MCU (STM32F103ZET6, STMicroelectronics, Switzerland), a steering stepper motor (60BEP115LC, Times Brilliant Electrical LLC, China), a steering motor driver (HBS86HAC, Times Brilliant Electrical LLC, China), a brushless direct current motor (86BL130-430, Times Brilliant Electrical LLC, China), and a brushless direct current motor driver (ZM6618, Times Brilliant Electrical LLC, China). The detailed specifications of the ultrasonic ridge-tracking

system components are listed in Table 2 and the schematic of the developed ultrasonic ridge-tracking system is shown in Figure 3.

Table 2. Specifications of the ultrasonic ridge-tracking system components.

Component	Manufacturer	Model	Function
Ultrasonic sensor	Shenzhen Dianyingpu Technology Ltd., Shenzhen, China	DYP-A02YY-V2.0	Monitoring the distance from ultrasonic sensor to the sidewall
PLC	Wuxi Xinjie Company Limited by share, Wuxi, China	XD3-32T-C	Controlling the rotational speed and rotational angle of the motors
MCU	STMicroelectronics, Geneva, Switzerland	STM32F103ZET6	Processing the measuring results and developed ultrasonic ridge-tracking algorithm
ESAS	Guangzhou Xingyi Electronic Co., Ltd., Guangzhou, China	ELITE	Integrating the peripheral circuit of the MCU
Steering stepper motor	Times Brilliant Electrical LLC, Beijing, China	60BEP115LC	Controlling the steering angle of the front wheels
Steering motor driver	Times Brilliant Electrical LLC, Beijing, China	HBS86HAC	Driving the stepper motor
Brushless direct current motor	Times Brilliant Electrical LLC, Beijing, China	86BL130-430	Powering the driving mechanism of the ridge transplanter
Brushless direct current motor driver	Times Brilliant Electrical LLC, Beijing, China	ZM6618	Driving the brushless direct current motor

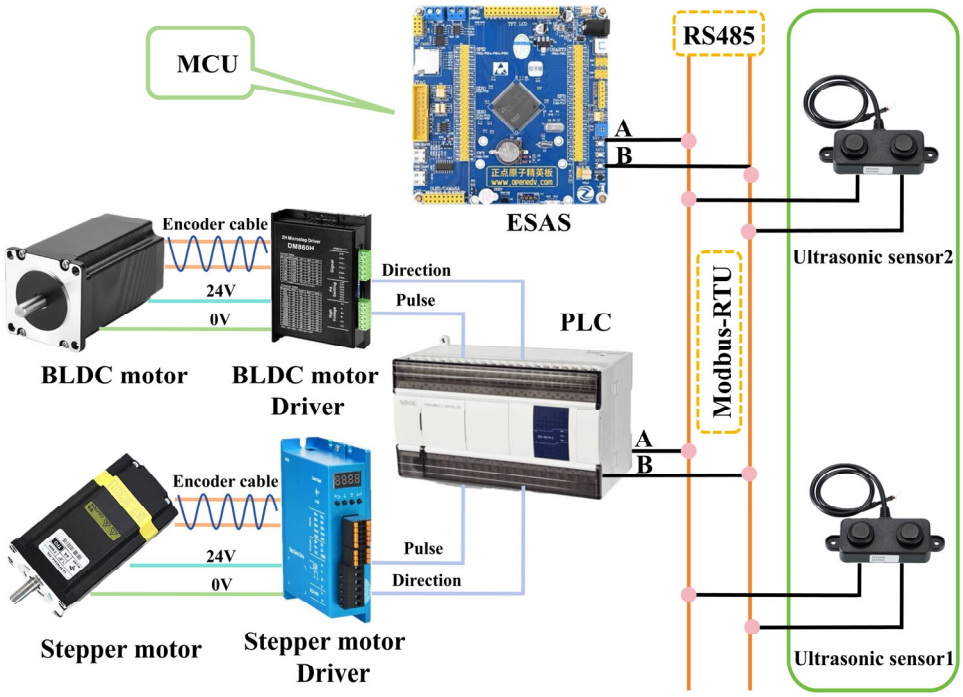

Figure 3. Components of the developed ultrasonic ridge-tracking system.

The ultrasonic sensors were used to measure the distances from the ridge sidewalls to the transplanter. The ESAS was applied to process the ultrasonic measurement information and operate the control algorithm. Then, the ESAS sent the rotational angle of the steering motor and the rotational speed of the driving motor into the PLC. The PLC controlled the rotational angle of the steering motor as well as the rotational speed of the driving motor by changing the frequency of the pulses. Moreover, the rotational directions of the steering

and driving motors were regulated by the different electronic level output by the PLC. The stepper motor was used to drive the steering mechanism and the brushless direct current motor was applied to drive the driving mechanism.

The hardware connection and the protocol from the ultrasonic sensors to the ESAS were the RS485 and the Modbus-RTU. The sample frequency of the ultrasonic sensor was 14 Hz. Moreover, the physical and protocol that connected the ESAS to the PLC were RS485 and Modbus-RTU protocol.

2.4. Principle of the Proposed Ultrasonic Ridge-Tracking Method

The principle of the proposed ultrasonic ridge-tracking method can be explained as follows. The ultrasonic sensors were used to measure the distance from the ultrasonic sensor to the ridge sidewall, and then the raw data were input into the limiter sliding window filtering algorithm to filter abnormal measuring results. After that, the center deviation was computed according to the distances from the ultrasonic sensors to the ridge sidewalls. In the next step, the optimal front sight point was selected from the optional ridge centers according to the current lateral deviation and traveling velocity. The look-ahead distance was equal to the norm of the vector from the center of the rear axle of the transplanter to the selected front sight point. According to the computed look-ahead distance, the steering angle model outputted the theoretical steering angle of the front wheels. After all of the above controlling processes were finished, the control process in the sampling period t was accomplished. The block diagram of the proposed URT method is demonstrated in Figure 4. The key innovations (i.e., the limiter sliding window filter and the fuzzy look-ahead distance decision model) are marked in red in Figure 4.

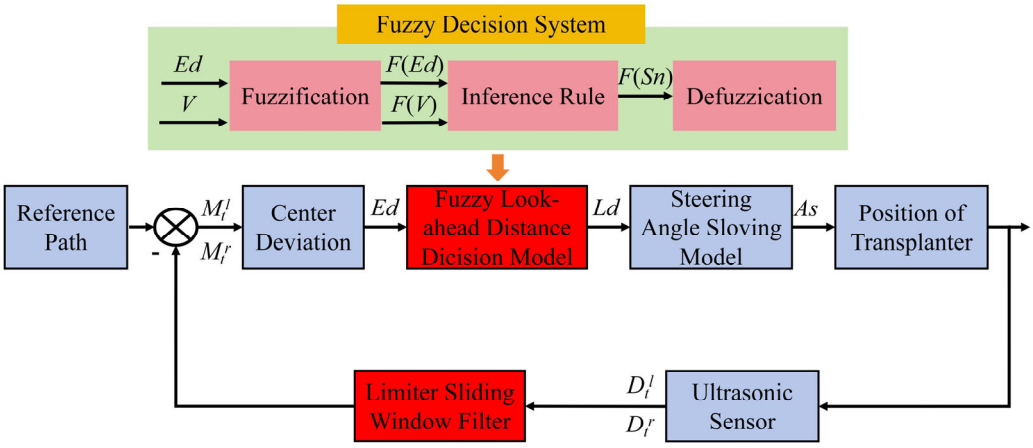

Figure 4. Block diagram of the proposed ultrasonic ridge-tracking method.

In Figure 4, $D_t{}^l$ and $D_t{}^r$ are the distances to the left and right ridge sidewalls at the sampling period t; $M_t{}^l$ and $M_t{}^r$ are the filtered measured distances to the left and right ridge sidewalls at sampling period t; Ed is the lateral deviation between the ridge center and transplanter center; V means the traveling velocity of the transplanter; $F(Ed)$, $F(V)$, and $F(Sn)$ denote the fuzzy membership of the lateral deviation, traveling velocity, and serial number of the optional ridge center, respectively; Ld denotes the optimal look-ahead distance; As means the theoretical steering angle of the front wheel.

2.5. Limiter Sliding Window (LSW) Filtering Algorithm

In order to acquire the deviation between the transplanter and the ridge, the distances from the two ridge sidewalls to the transplanter were measured by left and right ultrasonic sensors, respectively.

The transverse distance between the two ultrasonic sensors was 804 mm. In this research, the ridges for planting strawberry were selected as the application object. The width (i.e., the transverse distance between two vertical sidewalls) and height of the ridges

was 600 mm and 250 mm. If the transplanter center was misaligned with the ridge center, then the transverse distance from one sidewall of ridge to the ultrasonic sensor was more than 102 mm, and the transverse distance from the other side of ridge to the sensor was less than 102 mm. Regarding the height of the ultrasonic sensors, it should be lower than the height of ridge; thus, in this research, the installation height was set as 50 mm. The installation positions of the ultrasonic sensors are shown in Figure 5.

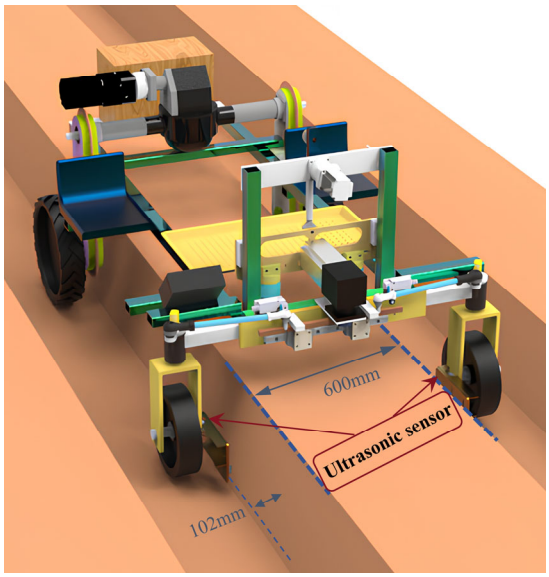

Figure 5. Installation positions of the ultrasonic sensors.

As the transplanter travels, the distance needs to be measured in real time from the ultrasonic sensor to the surface of the sidewall. The direction of the transplanter was determined by the left and right distances monitored by the ultrasonic sensors. If a sidewall of the ridge was damaged, the ultrasonic wave would not reflected on the surface but on the irregular pit of the sidewall, which may lead to malfunctions of the steering mechanism. For example, if the left sidewall was damaged, then the left ultrasonic sensor would obtain a large distance compared to the distance to the sidewall. Accordingly, the transplanter would judge that it was far away to the left sidewall, and then the steering mechanism would move to the right direction, as seen in Figure 6. After that, the center of the transplanter may offset in the right direction and the transplanter would travel in a wrong direction. In practice, the transplanter should monitor the distance to the sidewall rather than the local pits. Therefore, in order to reduce the influence of ridge damage, the limiter sliding window (LSW) filter was developed to filter the measured distances to the pits.

The limiter algorithm can effectively overcome the interference caused by accidental factors, and the sliding window algorithm can use several previous measuring results to smooth the final result. If the limiter algorithm and the sliding window algorithm can be fused, then the measuring distances at damaged pits can be removed and the several previous measuring distances can be used to obtain a precise measuring result. Therefore, the limiter sliding window (LSW) filtering algorithm was proposed in this study.

The processes of the LSW filtering algorithm will be explained as follows. The first step was a limiter process that was used to judge the range of the current measuring results. If the difference between the current measuring value D_t and the last measuring value D_{t-1} was less than the limiter threshold ΔT, then the current value D_t would be selected as the effect value. Otherwise, the last measuring value D_{t-1} was chosen as the effect value.

(**a**)

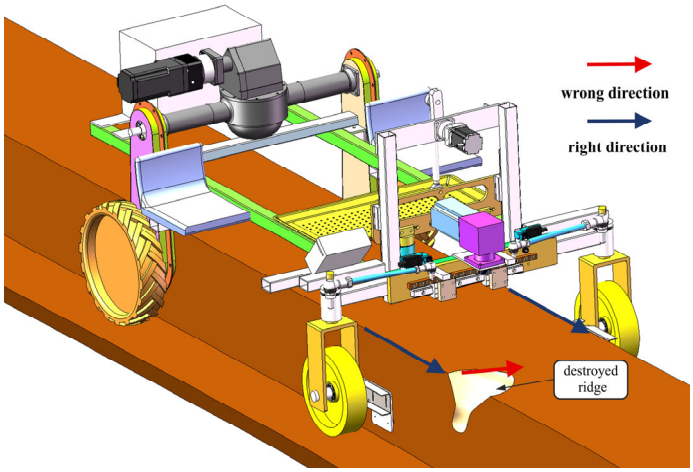

(**b**)

Figure 6. Direction change affected by the damaged ridge. (**a**) Actual damaged ridges; (**b**) malfunction caused by the damaged ridge.

The formula of the limiter process is listed below:

$$EV_t = \begin{cases} D_t & |D_t - D_{t-1}| \leq \Delta T \\ D_{t-1} & |D_t - D_{t-1}| > \Delta T \end{cases} \quad (1)$$

where EV_t implies the effect value of the limiter process at sampling period t, mm;

D_t denotes the measuring result at sampling period t, mm;

D_{t-1} denotes the measuring result at sampling period $t-1$, mm;

ΔT is the limiter threshold, in this study, ΔT was selected as 100 mm.

The second step was the sliding window process. The sliding window had 7 effect values from EV_{t-1} to EV_{t-7}. When the newest effect value EV_t was added to the sliding window, the oldest one EV_{t-7} would be removed from the sliding window.

The third step was the sorting process. The effect values in the sliding window were sorted by the bubble method. The fourth step was the removing process, in which the maximum and minimum in the sliding window were removed. The fifth step was solving for the average processing value, followed by computing the mean of the remaining 5 effect values as the consequence of the LSW filtering algorithm.

The equation of the LSW filtering algorithm can be illustrated as follows.

$$M_t = \frac{1}{TN-2} \times \left(\sum_{k=(t-6)}^{t} EV_t - Max - Min \right) \quad (2)$$

where TN indicates the total number of effect values in the sliding window. In this research, TN is equal to 7:

k represents the serial number of effect values in the sliding window;
EV_t implies the effect value of the limiter process at sampling period t, mm;
Max means the maximum of the elements in the sliding window, mm;
Min means the minimum of the elements in the sliding window, mm;
M_t is the filtered data in the sampling period t;
t implies the serial number of the sampling periods.
The schematic of the LSW filtering algorithm is illustrated in Figure 7.

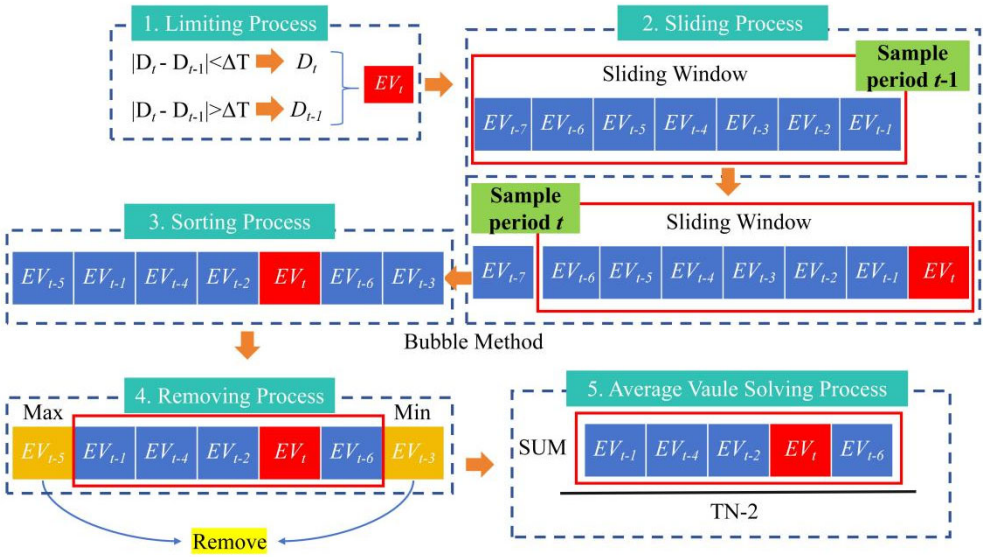

Figure 7. Schematic of the LSW filtering algorithm. The red block means the effect value at the current sample period t; the blue blocks denote the effect values in the previous sampling periods from $t-1$ to $t-7$; the yellow blocks are the max and min of the effect value sequence.

2.6. Kinematic Model of the Ridge Transplanter

In this research, the kinematic model of the ridge transplanter was the relationship between the position of front sight point and the theoretical steering angle of the front wheel. The norm of the vector from the center of the rear axle of the transplanter to the front sight point was defined as the look-ahead distance. In this study, the center in the width direction of the ridge, which was abbreviated as the ridge center, was viewed as the optional front sight point. Hence, it is important to obtain the accurate coordinates of the ridge centers. The measured ridge center at the sampling period t in the coordinate of the transplanter was $P_t(x_t, y_t)$, whose coordinates can be computed as follows.

$$D_l = S - M_t^l \quad (3)$$

$$D_r = S - M_t^r \quad (4)$$

where S is the theoretical distance between the ultrasonic sensor and the middle line of the transplanter, mm. In this study, S is equal to 402 mm.

$M_t{}^l$ is the filtered result between the left ultrasonic sensor and the left sidewall of ridge, mm;

$M_t{}^r$ is the filtered result between the right ultrasonic sensor and the right sidewall of ridge sidewall, mm;

D_l is the distance between the left sidewall and the ridge center, mm;

D_r is the distance between the right sidewall and the ridge center, mm.

The x-coordinate of the ridge center in the coordinate system of transplanter can be computed by Equation (5).

$$x_t = D_r - D_l = M_t^r - M_t^l \tag{5}$$

where x_t is the x-coordinate of the ridge center.

D_l is the distance between the left sidewall and the ridge center, mm;

D_r is the distance between the right sidewall and the ridge center, mm.

$M_t{}^l$ is the filter result between the left ultrasonic sensor and the left sidewall of the ridge, mm;

$M_t{}^r$ is the filter result between the right ultrasonic sensor and the right sidewall of the ridge, mm;

The y-coordinate of the ridge center was the distance between the center of the rear axle (i.e., the origin of the coordinate system of the transplanter) and the center of the two ultrasonic sensors. The exact value of the y-coordinate at a sampling period $t(y_t)$ was 1253 mm. The coordinate of the ridge center $P_t(x_t, y_t)$ is demonstrated in Figure 8.

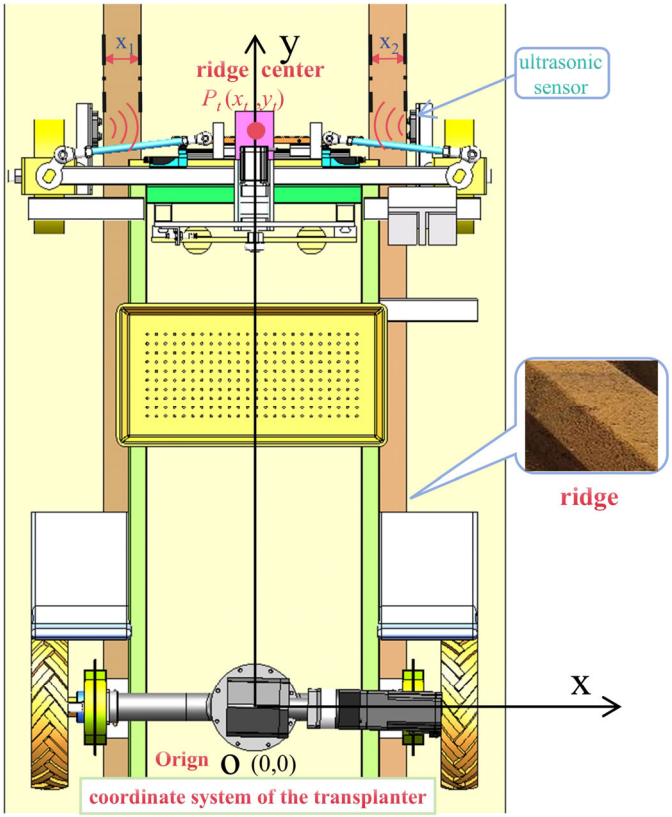

Figure 8. Coordinate of the ridge center in the coordinate system of transplanter.

As the transplanter traveled, the coordinates of ridge centers were updated. The coordinate of the nth ridge center $P_t{}^n(x_t{}^n, y_t{}^n)$ at sampling period t transformed into the $P^n{}_{t+1}$ $(x^n{}_{t+1}, y^n{}_{t+1})$ at sampling period $t + 1$, which is demonstrated in Equation (6).

$$\begin{bmatrix} x_{t+1}^n \\ y_{t+1}^n \\ 1 \end{bmatrix} = \begin{bmatrix} cos\phi & sin\phi & v \cdot t \cdot sin\phi \\ -sin\phi & cos\phi & v \cdot t \cdot cos\phi \\ 0 & 0 & 1 \end{bmatrix} \cdot \begin{bmatrix} x_t^n \\ y_t^n \\ 1 \end{bmatrix} \tag{6}$$

where v is the traveling velocity of the transplanter, mm/s.

φ is the difference of the heading angle of transplanter between the sampling period $t + 1$ and the sampling period t, rad;

n indicates the serial number of the ridge centers.

The schematic of the coordinate transform of the ridge centers is illustrated in Figure 9.

$$n = \frac{y_t}{V} \tag{7}$$

where n denotes the total number of the optional ridge centers.

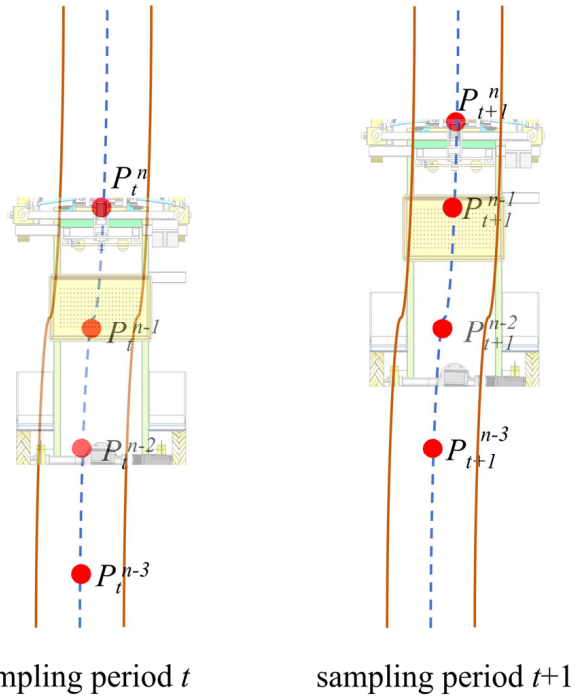

Figure 9. Coordinate transform of ridge centers.

y_t means the distance between the center of the rear axle to the center of the two ultrasonic sensors, mm;

V indicates the traveling velocity of the transplanter, mm/s.

If a new ridge center was added to the optional queue, then the oldest one was discarded. According to Equation (6), when the transplanter at sampling period t moved to a new position at sampling period $t + 1$, the coordinates of the ridge centers in the optional queue (from ${P_t}^1$ to ${P_t}^n$) were updated to the new coordinates (from ${P^1}_{t+1}$ to ${P^n}_{t+1}$).

Moreover, the kinematic model of the transplanter can be simplified as a two-wheel model, as seen in Figure 10. In addition, the relationship between the look-ahead distance, turning radius, and angle deviation of the two-wheel model is demonstrated in Equation (8).

$$\frac{l_d}{sin(2\alpha)} = \frac{R}{sin(\frac{\pi}{2} - \alpha)} \tag{8}$$

where l_d is the look-ahead distance, mm.

R represents the turning radius, mm;

α denotes the heading deviation, rad.

Equation (8) can be simplified as the following Equation (9)

$$\frac{1}{R} = \frac{2 \times sin\alpha}{l_d} \tag{9}$$

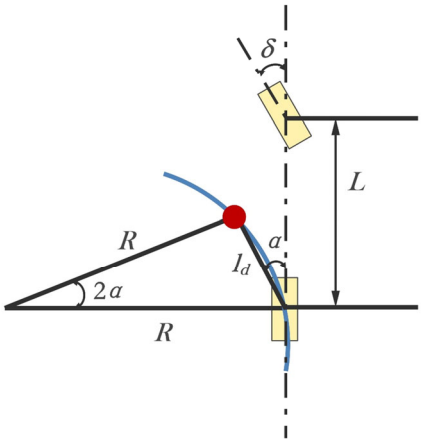

Figure 10. Two-wheel model of the ridge transplanter. L indicates the wheel base of the transplanter; α is the heading deviation; δ represents the steering angle of the front wheel; R means the turning radius, and L_d denotes the look-ahead distance.

So as to ensure that the center of the rear axle can overlap with the selected front sight points, the front wheel steering angle must be controlled. The steering angle of the front wheel can be computed by Equation (10).

$$\delta = arctan\frac{L}{R} \tag{10}$$

where δ represents the steering angle of front wheel, rad.

L indicates the wheel base of the transplanter, mm;

R represents the turning radius, mm.

Substituting Equation (9) into Equation (10), the steering angle of the front wheel can be deduced as Equation (11) [24].

$$\delta = \arctan\left(\frac{2 \times L \times sin\alpha}{l_d}\right) \tag{11}$$

According to Equation (11), the front wheel steering angle was determined by the wheel base, look-ahead distance, and heading deviation. Because the sampling period was short and the traveling velocity was slow, the heading deviation between two continuous sampling periods was viewed as the same, so that the influence of the heading deviation can be neglected. The heading deviation from the center of the rear axle to the front sight point can be expressed by Equation (12).

$$\alpha = arcsin\left(\frac{M_t^r - M_t^l}{l_d}\right) \tag{12}$$

where $M_t{}^l$ is the filtered result between the left ultrasonic sensor to the left sidewall of ridge, mm.

$M_t{}^r$ is the filtered result between the right ultrasonic sensor to the right sidewall of ridge, mm;

l_d is the look-ahead distance, mm.

Substituting Equation (12) into Equation (11), the steering angle model can be calculated by Equation (13).

$$\delta = \arctan\left[\frac{2 \times L \times \left(M_t^r - M_t^l\right)}{{l_d}^2}\right] \tag{13}$$

Equation (13) shows that the front wheel steering angle was determined by the wheel base, left ridge distance, right ridge distance, and look-ahead distance. Both of the left ridge distance and right ridge distance can be measured by the ultrasonic sensors. According to the aforementioned steering angle model, the look-ahead distance was the only variable to be determined.

2.7. Fuzzy Look-Ahead Distance Decision Model

In this research, the optimal front sight point was selected from the optional ridge centers measured in the latest n sampling periods. The total number of ridge centers in the optional queue can be computed by Equation (8). When the look-ahead distance was short, the lateral adjustment ability was enhanced and the transplanter quickly approached the front sight point with a large curvature. However, a short look-ahead distance led to the trajectory-tracking oscillation when approaching the front sight point. When the look-ahead distance was long, the transplanter slowly approached the reference path with a small curvature. Under such a condition, the tracking route did not oscillate, but the adjustment time was longer. Therefore, according to the above analyses, the look-ahead distance needs to be regulated according to different lateral deviation conditions.

As for the relationship between the traveling velocity and look-ahead distance, if the traveling velocity of the transplanter was large, then the look-ahead distance should become large in order to improve the stability in the tracking process. In contrast, if the velocity of the transplanter was low, then the look-ahead distance should be small to improve the precision of tracking.

According to the analyses above, the lateral deviation and the traveling velocity were used as the factors for deciding the look-ahead distance. Based on different lateral deviations and velocities, a fuzzy look-ahead distance decision model was proposed to determine the appropriate look-ahead distance. The inputs of the fuzzy look-ahead decision method were the lateral deviation and traveling velocity. Additionally, the output of the fuzzy look-ahead decision model was the serial number of the front sight points. In the next step, the look-ahead distance can be computed by the norm of the vector from the center of the rear axle (the original of the coordinate system of the transplanter) to the selected front sight point, which is listed in Equation (14).

$$l_d = \sqrt{\left(x_t^k\right)^2 + \left(y_t^k\right)^2} \tag{14}$$

where l_d denotes the look-ahead distance, mm.

${x_t}^k$ implies the x-coordinate of the kth ridge center at the sampling period t, mm;

${y_t}^k$ implies the y-coordinate of the kth ridge center at the sampling period t, mm;

k means the serial number of selected front sight point;

t means the current sample period.

The distance between the two ultrasonic sensors was 804 mm and the width of the standard ridge was 600 mm. If one side of the transplanter contacted the ridge sidewall, then the maximum lateral deviation was 204 mm. According to above analyses, the basic domain of the lateral deviation was set as {0 mm, 210 mm}. As for the traveling velocity, the universal traveling velocity range of the ridge transplanter was from 37.5 mm/s to 62.5 mm/s, so the range {30 mm/s, 70 mm/s} was set as the basic domain of the traveling velocity.

The longitudinal separation from the center of ultrasonic sensors to the center of the rear axle was 1250 mm. So as to leave transplanter enough distance to regulate, the smallest serial number of the optional front sight points was chosen as 10th. If the transplanter traveled at velocity of 37.5 mm/s, then the max serial number of optional front sight points was 33rd. Therefore, the basic domain of the serial number of the optional front sight points was {10, 30}. The membership functions of the lateral deviation, traveling velocity, and serial number of optional front sight points were triangular, as shown in Figure 11.

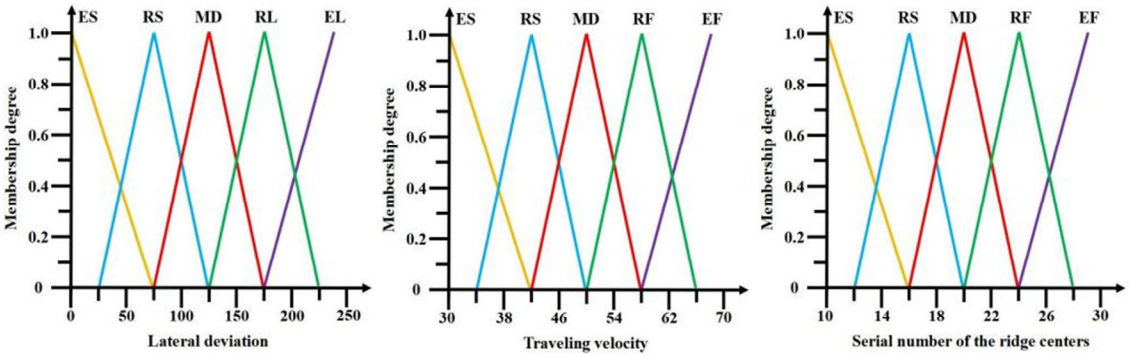

(**a**) (**b**) (**c**)

Figure 11. Membership function distributions of the lateral deviation, traveling speed, and serial number of front sight points. (**a**) The membership function of the lateral deviation; (**b**) the membership function of the traveling speed; (**c**) the membership function of the serial number of front sight points.

The fuzzy sets of lateral deviations were classified as {ES (extremely small), RS (relatively small), MD (medium), RL (relatively large), and EL (extremely large)}. The fuzzy sets of the travel velocity were classified as {ES (extremely slow), RS (relatively slow), MD (medium), RF (relatively fast), and EF (extremely fast)}. The fuzzy sets of the serial number of the optional front sight points were classified as {ES (extremely small), RS (relatively small), MD (medium), RL (relatively large), and EL (extremely large)}. The inference rules used to obtaining the optimal serial number of the front sight points are listed in Table 3.

Table 3. Fuzzy inference rules for the optimal serial number of the front sight points.

Serial Number of Front Sight Points		Traveling Velocity				
		ES	**RS**	**MD**	**RF**	**EF**
Lateral Deviation	ES	RL	RL	EL	EL	EL
	RS	MD	MD	RL	EL	EL
	ZO	RS	RS	MD	RL	RL
	RL	ES	RS	MD	MD	MD
	EL	ES	ES	ES	RS	RS

The centroid method was used to defuzzification of the serial number of the front sight points. If the consequence of the defuzzification was a decimal, the rounding-off method was applied to round up the decimal. After obtaining the serial number of the front sight points, the look-ahead distance and the front wheel steering angle were calculated by Equations (13) and (14).

2.8. Field Experiments

2.8.1. Validation Experiment of the LSW Filtering Algorithm

The premise of accurate ridge tracking was to obtain the precise lateral deviation between the transplanter and ridge. Thus, a full factorial experiment was conducted to compare the performance of the proposed LSW filtering algorithm and the commonly used direct measuring method.

The theoretical measuring distance and traveling velocity of the ridge transplanter were selected as the experimental factors. Under each factorial combination, the experiment was repeated three times. The top width, bottom width, and height of the ridge were 400 mm, 600 mm, and 300 mm, respectively. The theoretical measuring distance between the ultrasonic sensor and the ridge sidewall was set manually at the start point and then the transplanter traveled forward automatically. The picture of the validation experiment of the LSW filtering algorithm is displayed in Figure 12.

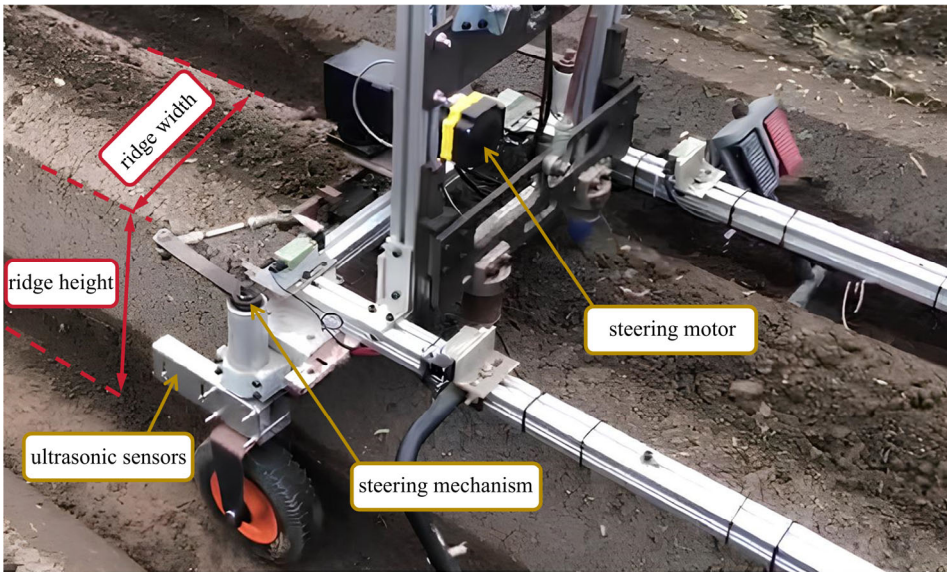

Figure 12. Validation experiment of the LSW filtering algorithm.

According to the actual velocity range of the ridge transplanter, the experimental levels of traveling velocity were 37.5 mm/s, 50 mm/s, and 62.5 mm/s. Moreover, the factorial levels of the theoretical measuring distance were 30 mm, 90 mm, 150 mm, and 210 mm. The indicator of the validating experiments was the mean absolute percentage error (MAPE), which can be calculated according to Equation (15).

$$\mathrm{MAPE} = \frac{1}{N} \cdot \sum_{i=1}^{N} \left[\left| \frac{\mathrm{TD} - MD_i}{\mathrm{TD}} \right| \times 100\% \right] \tag{15}$$

where MAPE represents mean absolute percentage error, %.

TD means theoretical measuring distance, mm;

MD_i indicates the measuring distance, mm;

i is the serial number of repetitions;

N is the repetition of each level combination; in this study, N is equal to 3.

2.8.2. Comparison Experiment of the Proposed Ultrasonic Ridge-Tracking (URT) Method and the Universal Pure Pursuit (UPP) Method

In order to test the performance and robustness of the proposed URT method and the universal pure pursuit (UPP) method, field experiments were conducted. The experimental greenhouse is named DaXiaoHua family farm (119.34° E, 31.98° N) and is located in Jurong city, Jiangsu province. The top width, bottom width, height, and length of the experimental ridge was 400 mm, 600 mm, 250 mm and 50 m, respectively.

The traveling velocity of the transplanter was regarded as the experimental factor, and the experimental levels of the forward velocity were 37.5 mm/s, 50 mm/s and 62.5 mm/s. At each experimental level, the transplanter traveled 20 m.

Moreover, the lateral deviation was used as the experimental index to judge the performance of the proposed URT method and conventional UPP method. The URT method used the variable look-ahead distances and the conventional UPP method applied the current measured ridge center as the front sight point. The procedures of the experiment of the proposed ridge-tracking system are demonstrated below.

Before the test, red liquid dye was added to a container that had a hole in its cap. Then, the container was fixed to the center of the rear axle of the transplanter. Additionally, the traveling velocity on human machine interface was set. When the transplanter traveled along the ridge, a red line of transplanter trace was formed on the top surface of the

experimental ridge. The red trace line was the projection of the transplanter center on the ridge top.

After each experiment, ten ridge centers were measured with an interval of 100 mm at the start points of 0 m, 5 m, 10 m, and 15 m. The schematic of the whole experimental route is shown in Figure 13. The centers of the ridge top surface were marked with green dye. The deviation between the green markers and the red track line were measured by a vernier caliper with a precision of 0.01 mm. Then, the lateral deviation between the trace of the transplanter and the ridge centers was obtained. In order to validate the deviation correction capability of the two tracking methods, the center of the transplanter was set to deviate 50 mm from that of the ridge at the starting point. The field experiment of the proposed URT method and conventional UPP method is illustrated in Figure 14.

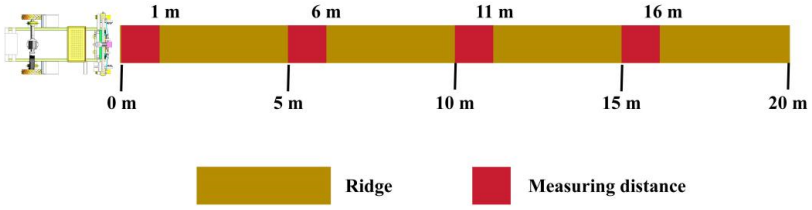

Figure 13. The measuring positions along the ridge.

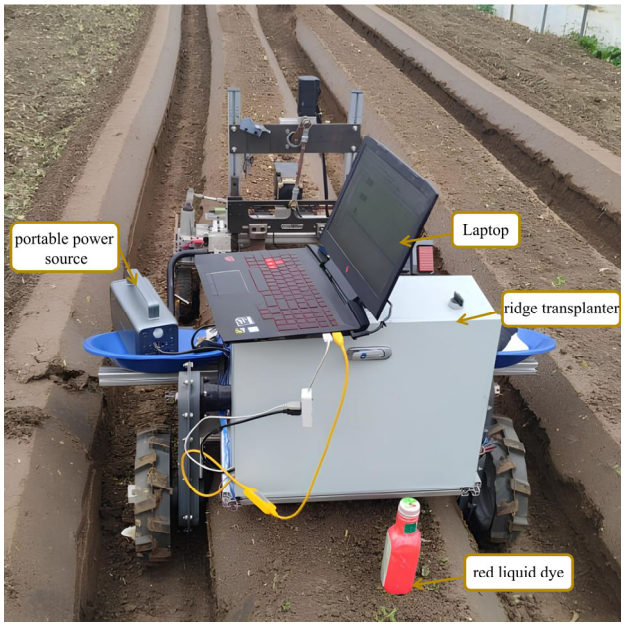

Figure 14. Validation experiment of the URT method.

Furthermore, the indicators of the validation experiment were mean absolute lateral deviation (MALD), maximum absolute lateral deviation (MXALD), and root mean square lateral deviation (RMSLD). The formulas of the MALD and RMSLD are listed in Equations (16) and (17).

$$\mathrm{MALD} = \frac{1}{N} \cdot \sum_{i=1}^{N} |E_i| \tag{16}$$

$$\mathrm{RMSLD} = \sqrt{\frac{1}{N} \cdot \sum_{i=1}^{N} (E_i)^2} \tag{17}$$

where MALD is the mean absolute lateral deviation, mm.

RMSLD denotes the root mean square lateral deviation, mm;

N means the total number of lateral deviations;

E_i is the lateral deviation between the trance of transplanter and the ridge center, mm;

i implies the serial number of the lateral deviations.

3. Results

3.1. Performance Comparison between the LSW Filtering Method and the Direct Measuring Method

The final results of the LSW filtering method and the direct measuring method are displayed in Table 4 and the average values of the final results are displayed in Figure 15. Because the raw outputs of the ultrasonic sensor were integrals, the final results of the direct measuring method were also integrals. Moreover, the final results of the LSW filtering method were decimals because they were the average value of the data in the sliding window. The ranges of the absolute measuring errors of the LSW filtering method and the direct measuring method were 0.6 mm~5.4 mm and 1 mm~7 mm.

Table 4. The final results of the LSW filtering method and direct measuring method.

Theoretical Distance (mm)	Velocity (mm/s)	Final Results (mm)		Theoretical Distance (mm)	Velocity (mm/s)	Final Results (mm)	
		LSW Filtering Method	Direct Measuring Method			LSW Filtering Method	Direct Measuring Method
30	37.5	31.4	31	90	37.5	87.8	86
		31.6	32			92.4	93
		30.8	31			88.2	87
	50	30.6	32		50	93.2	95
		31.4	30			92.4	94
		31.2	31			87.6	88
	62.5	31.2	32		62.5	87.4	87
		31	31			93.4	94
		32.2	32			93.6	95
150	37.5	148.6	148	210	37.5	206.8	205
		152.8	153			207.4	214
		153.8	155			212.6	213
	50	153.4	145		50	213.6	214
		146.4	151			215.4	215
		148.6	147			208.2	206
	62.5	152.8	153		62.5	206.2	203
		154.6	147			216.4	214
		148.8	154			208.2	206

In most cases, the final results of the LSW filtering method were closer to the theoretical measuring distance. However, under the theoretical measuring distance of 30 mm and the traveling velocity of the 50 mm/s, the final result of the direct measuring method was equal to 30 mm, leading to a more accurate average and a lower MAPE value. The reason might be that the dead zone of the ultrasonic sensor was 0 mm~30 mm, and if the measuring distance was less than 30 mm, then the outputs of the ultrasonic sensor were saturated and the output was 30 mm. When conducting the experiment, the distance between the ultrasonic sensor and the sidewall of the ridge might be less than 30 mm, so the output of the ultrasonic was 30 mm.

Under each combination of the levels of factors, the MAPE of the LSW filtering method and direct measuring method are demonstrated in Figure 16. The range of the MAPE of the LSW filtering method was from 1.33% to 4.89%, and that of the direct measuring method was from 1.90% to 5.56%.

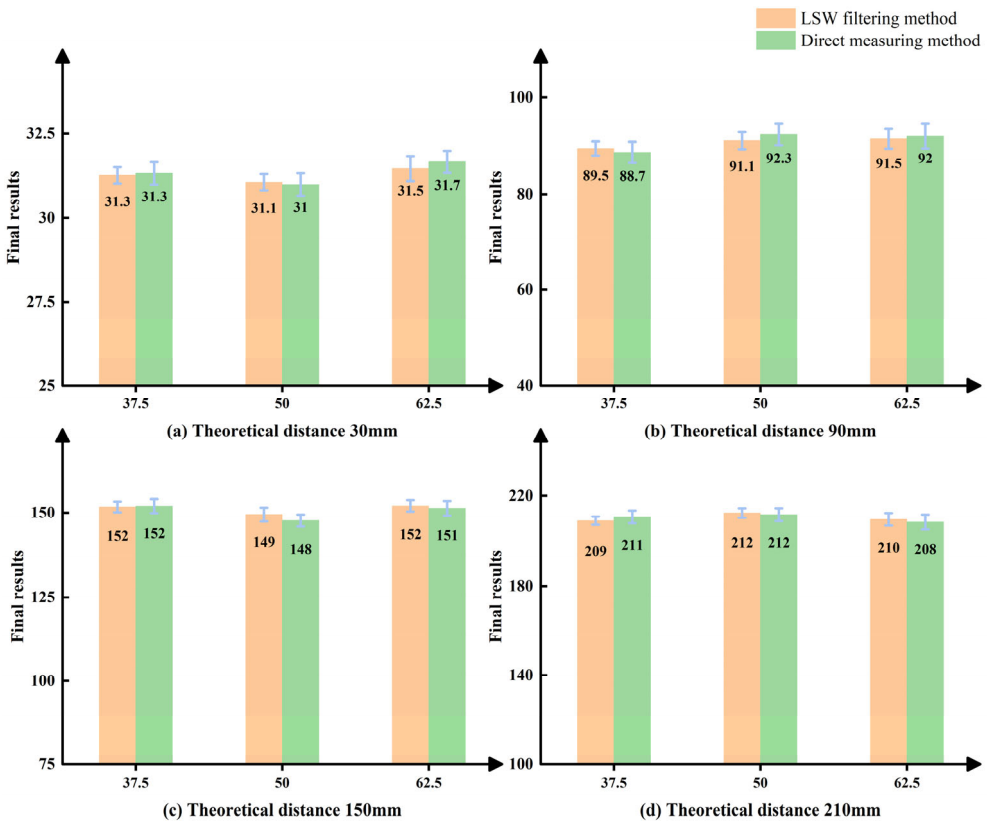

Figure 15. Average value of the final results of the LSW filtering method and the direct measuring method.

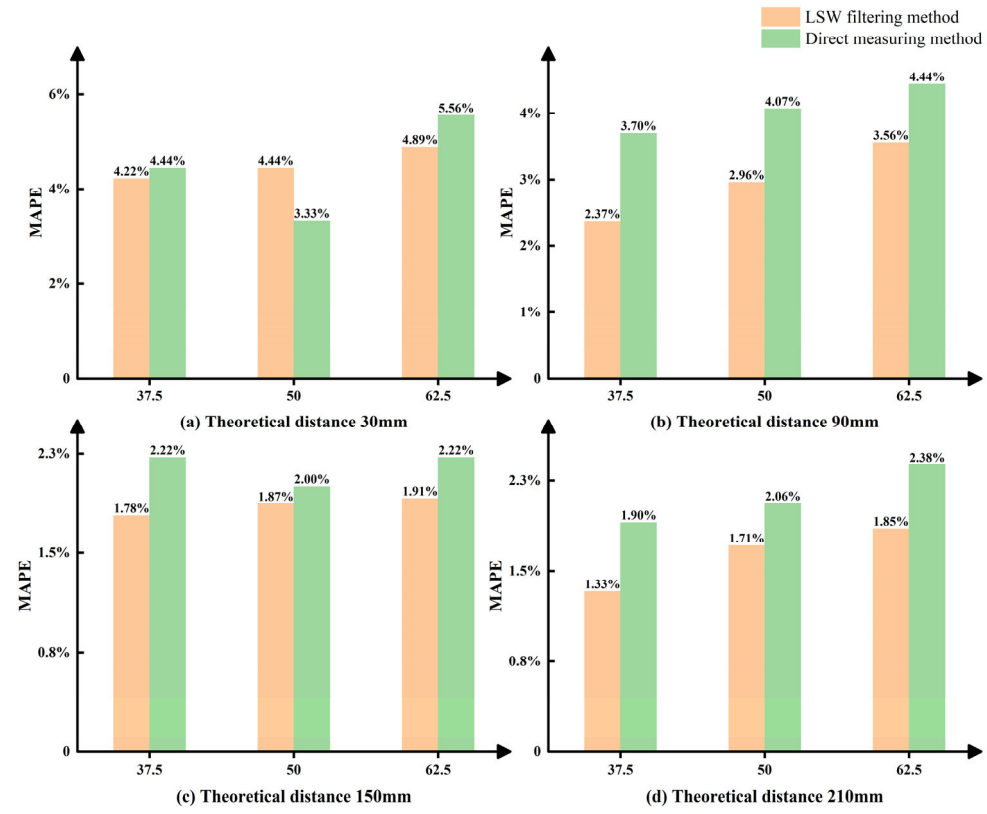

Figure 16. MAPE of the LSW filtering method and the direct measuring method.

As seen in Figure 16, when the theoretical measuring distance was the same, the MAPE of both measuring methods also rose as the traveling velocity increased, but the differences were not obvious. The velocity of the ultrasonic wave was greater than the traveling velocity of the transplanter, so the traveling velocity of the transplanter was not a significant factor in the accuracy of the final results.

As the theoretical measuring distance increased, the trend of the MAPE of both methods decreased at the same traveling velocity. As the theoretical measuring distance increased, the MAPE of both methods decreased, although the absolute errors of the final results increased. Because the measuring errors of the ultrasonic sensor were within a certain range, the relative error rate was lower as the theoretical measuring distance increased.

Under each combination of the levels of factors, the MAPE of the LSW filtering method was less than that of the direct measuring method. The reason is analyzed below. The raw outputs of the ultrasonic sensor had random measuring noise. The direct measuring method used the raw outputs as the measuring results, and hence the final results also had the random noise. Regarding to the LSW filtering method, the largest and the smallest measuring data in the sliding window were removed and the average value of the remaining data were reviewed as the final measuring result. According to the above analysis, the positive random measuring noise and negative ones were counteracted in the average solving process, which led to the final results with less random noise. That was the reason why the measuring performance of the proposed LSW filtering method was better than that of the direct measuring method.

3.2. Tracking Performance of the Proposed URT Method and the UPP Method

After each experiment, the traveling trajectory (red line) of transplanter was acquired and the ridge centers (green points) were measured, which is shown in Figure 17.

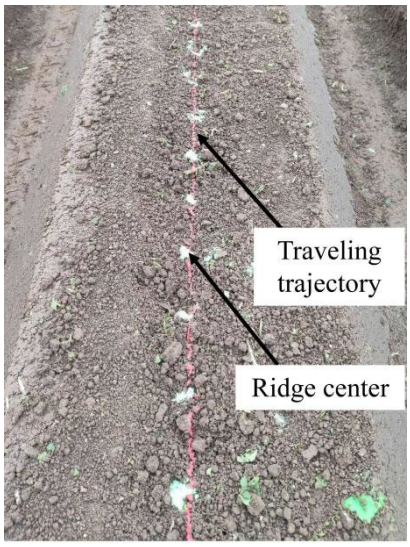

Figure 17. The marks of the traveling trajectory and ridge centers.

When the transplanter traveled at different velocities, the trend of the lateral deviations of the proposed URT method and conventional UPP method are shown in Figure 18. Positive lateral deviation meant the transplanter skewed to the right direction and negative lateral deviation meant the chassis skewed to the left direction. When the traveling distance exceeded 5 m, the transplanter was viewed as traveling in the steady state. At the traveling velocity of 37.5 mm/s, 50 mm/s, and 62.5 mm/s, the steady-state lateral deviations of the URT method were in the range of 1.25 mm~12.44 mm, 1.66 mm~14.74 mm, and 2.35 mm~18.87 mm, respectively; the steady-state lateral deviations of the UPP method ranged from 2.74 mm to 18.55 mm, 3.29 mm to 19.54 mm, and 3.24 mm to 23.23 mm, respectively.

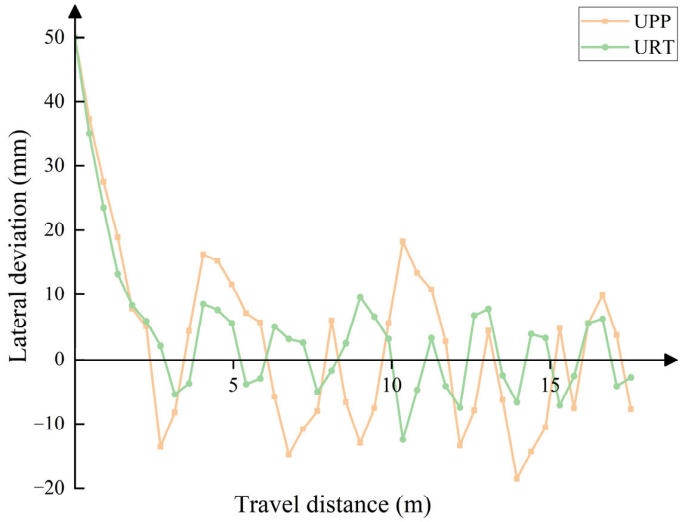

(**a**)

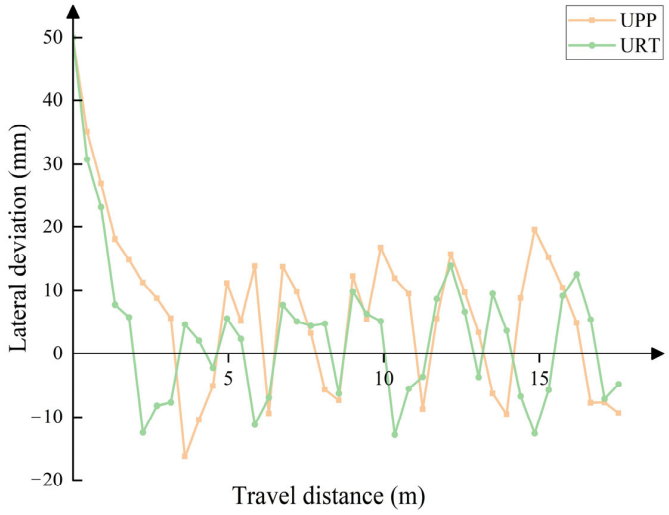

(**b**)

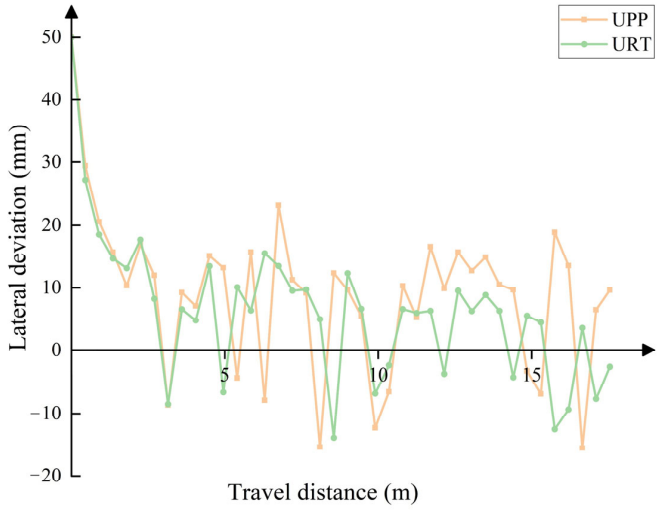

(**c**)

Figure 18. The lateral deviations controlled by the URT method and UPP method. (**a**) Lateral deviations at traveling velocity of 37.5 mm/s. (**b**) Lateral deviations at traveling velocity of 50 mm/s. (**c**) Lateral deviations at traveling velocity of 62.5 mm/s.

The MALD, MXALD, and RMSLD of the proposed URT method and conventional UPP method are shown in Table 5. When traveling at the same velocity, the MALD, MXALD, and RMSLD were less than their corresponding indicators in the UPP method, respectively. No matter the URT method or the UPP method, the MALD value at the traveling velocity of 62.5 mm/s was the highest, and that at the traveling velocity of 37.5 mm/s was the lowest. The MXALD values and RMSLD values also conformed to the same trend. The experimental results show that as the traveling velocity rose, the tracking performance of both of the URT method and the UPP method declined.

Table 5. The ridge-tracking indicators of the URT method and the UPP method.

Traveling Velocity (mm/s)	MALD (mm)		MXALD (mm)		RMSLD (mm)	
	URT	UPP	URT	UPP	URT	UPP
37.5	7.39	11.67	12.44	18.55	11.85	15.05
50	8.96	11.35	14.74	19.54	12.56	14.61
62.5	10.56	13.11	18.87	23.23	13.52	15.66

The reason why the faster the velocity, the worse the ridge-tracking performance will be analyzed. In the same sampling period, if the velocity was faster, then the transplanter traveled a longer distance compared to that at a low velocity. According to the tangent triangle function, the same heading error at a high velocity resulted in a significant lateral deviation because the hypotenuse was greater. Moreover, under the high-velocity condition, the traveling direction of a transplanter was more likely to be affected by the vibrations from the ground. The aforementioned two reasons may mean that the lateral deviations at a high velocity were greater than those at a low velocity.

4. Discussion

4.1. Tracking Performance Comparison

The curvature of the ridge is approximately a straight line, and thus some trajectory-tracking methods for straight line were compared to the research outcomes of Yang et al. [24], Hu et al. [25], and Zhang et al. [26] in Table 6, all of whom focused on path-tracking control for agriculture machinery. The proposed URT method exhibited significant advantages in both MALD and MXLD. Furthermore, it cannot be ignored that the previous results traveled along straight paths on a plat field, which made it much less difficult to follow the ridge. According to the above comparisons, the developed ultrasonic ridge-tracking method in this research had a desirable tracking performance in the ridge condition.

Table 6. Comparison between the developed URT method to previous route-tracking methods of agricultural machinery.

Tracking Method	Mean Absolute Lateral Deviation (mm)	Maximum Absolute Lateral Deviation (mm)
Developed URT method	8.42	18.87
Yang et al. [24]	18	46
Hu et al. [25]	35.4	127.2
Zhang et al. [26]	88	32

4.2. Strengths of the Proposed Ultrasonic Ridge-Tracking Method

In order to allow for seedlings with a certain row space and seedling space, the ridge transplanter should be able to track along the ridge. Some sensors, like GPS, cannot detect the position of the ridge, while machine vision or LiDAR would be affected by hard light in agricultural conditions. In order to overcome the mentioned sensing problems, the developed ridge-tracking method in this research used ultrasonic sensors to monitoring the relative position between the ridge and the transplanter. The robustness of the ultrasonic sensor was the great compared to machine vision and LiDAR. The key innovations of

the proposed URT method were the LSW filtering algorithm and the optimal look-ahead distance decision model. The strengths of the LSW filtering algorithm and the optimal look-ahead distance decision model are listed below.

1. The ridge damage phenomenon results in erroneous judgement of the steering angle. However, the proposed LSW filtering algorithm can filter the rapidly changing data, which probably represent the distances from the ultrasonic sensor to the ridge pits. Additionally, the proposed LSW method can improve the accuracy by fusing the measurement results from previous sampling periods. Hence, the tracking performance of the proposed URT method would not be obviously affected by ridge damage.
2. The conventional UPP method uses a certain look-ahead distance to determine the fore sight points, which may lead to a long regulating time under sizeable lateral deviation conditions or oscillations in the small lateral deviation conditions. The proposed URT method regulates the optimal look-ahead distance based on the actual lateral deviations and velocities, so the transplanter can keep a desirable ridge-tracking performance in real time.

4.3. Implication

The proposed URT method can not only be applied to the ridge transplanter, but also to other ridge-operation machinery, such as the harvester, seeder, and so forth. In other fields, the proposed tracking method can also be used in situations where robots or machinery move along a solid object below the chassis. For example, in logistics warehouses, transport robots can use the proposed tracking method to track the invariable route, which uses solid cuboid as the reference path.

4.4. Weaknesses and Future Research

Although the proposed URT method had ideal tracking performance when traveling along ridges, it is still a challenging operation to automate in ridge conditions. Ssymmetrical ultrasonic sensors can only monitor the distances to the ridge currently being tracked; that is to say, only the relative position between the operating ridge to the transplanter can be acquired. The relative position from the transplanter to the other ridges cannot be obtained. When traveling at the end of the ridges, the transplanter needs to be stopped and moved to an adjacent unoperated ridge manually.

The automatic level of the proposed URT method could be improved if the following suggestions are accepted in the future.

When a transplanter completes the operation on the current ridge, it needs to move off the current ridge and move on to an adjacent one. In future work, the URT system could fuse other sensing information to detect adjacent ridges. Based on the above system, the simultaneous location and mapping (SLAM) method of the ridge transplanter could be developed in the future.

Using the proposed URT method, the coordinates of the ridge centers obtained in previous sampling periods need to be transformed into the current coordinate system at the current sampling period by the coordination transform method. Thus, the position of the transplanter in the current sampling period relative to the previous sampling period is crucial. If the Kalman filter is used for estimating the positions and postures of the transplanter, then the coordinate transform of the ridge centers might be more accurate, which could result in a better tracking performance.

5. Conclusions

The main successes in this research were the development of an ultrasonic ridge-tracking method and its corresponding system for the ridge transplanter. The LSW filtering method was proposed to improve the accuracy of the ultrasonic measuring results and remove the abnormal values. Moreover, the fuzzy look-ahead distance decision model was developed to determine the optimal look-ahead distance in real time. The validation experiment of the proposed LSW filtering method was conducted. Additionally, the

tracking performances of the proposed URT method and the conventional UPP method were compared under field conditions.

With the same combination of factorial levels, the performance of the LSW filtering method was better than that of the direct measuring method. The MAPE values of the LSW filtering method and the direct measuring method were less than 4.89% and 5.56%. All of the MAPE values of the proposed LSW filtering method were less than 5%, and therefore the LSW filtering method was recommended to obtain the distances from the sidewalls to the ultrasonic sensors.

At different traveling velocities, the tracking performance of the URT method and that of the UPP method were compared. The greatest MALD values of the lateral deviations of the URT method and the UPP method were 10.56 mm and 13.11 mm. The greatest MXALD values of the lateral deviations of the URT method and the UPP method were 18.87 mm and 23.23 mm. Moreover, the greatest RMSLD values of the lateral deviations of the URT and the UPP were 13.52 mm and 15.66 mm. The experimental results showed that under the same combination of factorial levels, the tracking performance of the proposed URT method was better than that of the conventional UPP method.

According to the ridge-tracking performance of the proposed URT method, it can be used in practical agricultural ridge conditions, for example, transplanting, seeding, harvesting, and so on. Moreover, in other fields, robots or intelligent machinery can also apply the proposed URT method to track objects similar to ridges.

Author Contributions: Conceptualization, W.L. and J.Z.; methodology, W.L., M.Y. and Y.L.; software, W.L. and J.C.; validation, T.Z. and J.H.; formal analysis, W.L., J.H. and X.C.; investigation, M.Y. and T.Z.; resources, J.H.; data curation, W.L. and J.Z.; writing—original draft preparation, W.L.; writing—review and editing, W.L., C.Z. and J.H. All authors have read and agreed to the published version of the manuscript.

Funding: This work was supported by the Shanghai Agricultural Science and Technology Innovation Project "Research and Development of Key Intelligent Technologies for Fully Automated Lettuce Transplanting Equipment (2023-02-08-00-12-F04592)", the Priority Academic Program Development of Jiangsu Higher Education Institutions (no. PAPD-2023-87) and National Natural Science Foundation of China (Grant number 31901455).

Institutional Review Board Statement: Not applicable.

Data Availability Statement: Data are contained within the article.

Conflicts of Interest: The authors declare no conflict of interest.

References

1. Li, J.; Shang, Z.; Li, R.; Cui, B. Adaptive Sliding Mode Path Tracking Control of Unmanned Rice Transplanter. *Agriculture* **2022**, *12*, 1225. [CrossRef]
2. Fu, D.; Chen, Z.; Yao, Z.; Liang, Z.; Cai, Y.; Liu, C.; Tang, Z.; Lin, C.; Feng, X.; Qi, L. Vision-based trajectory generation and tracking algorithm for maneuvering of a paddy field robot. *Comput. Electron. Agric.* **2024**, *226*, 109368. [CrossRef]
3. Zhang, T.; Zhou, J.; Liu, W.; Yue, R.; Yao, M.; Shi, J.; Hu, J. Seedling-YOLO: High-Efficiency Target Detection Algorithm for Field Broccoli Seedling Transplanting Quality Based on YOLOv7-Tiny. *Agronomy* **2024**, *14*, 931. [CrossRef]
4. Tang, L.; Yan, F.; Zou, B.; Wang, K.; Lv, C. An Improved Kinematic Model Predictive Control for High-Speed Path Tracking of Autonomous Vehicles. *IEEE Access* **2020**, *8*, 51400–51413. [CrossRef]
5. Zhong, S.; Peng, D.; Huang, B.; Ma, L. Path-Tracking Ability of the ASV on Different Adhesion Coefficient Roads Based on Slide Mode Control. *Electronics* **2024**, *13*, 105. [CrossRef]
6. Cheng, J.; Zhang, B.; Zhang, C.; Zhang, Y.; Shen, G. A model-free adaptive predictive path-tracking controller with PID terms for tractors. *Biosyst. Eng.* **2024**, *242*, 38–49. [CrossRef]
7. Shi, Y.; Chen, X.; Xi, X.; Shan, X.; Jin, Y.; Zhang, R. Research progress on the path tracking control methods for agricultural machinery navigation. *Trans. Chin. Soc. Agric. Eng. (Trans. CSAE)* **2023**, *39*, 1–14.
8. Ahn, J.; Shin, S.; Kim, M.; Park, J. Accurate Path Tracking by Adjusting Look-Ahead Point in Pure Pursuit Method. *Int. J. Automot. Technol.* **2021**, *22*, 119–129. [CrossRef]
9. Xia, Q.; Chen, L.; Xu, X.; Cai, Y.; Jiang, H.; Pan, G. Expected yaw rate–based trajectory tracking control with vision delay for intelligent vehicle. *Sci. Prog.* **2020**, *103*, 1–23. [CrossRef]

10. Xu, S.; Peng, H.; Tang, Y. Preview Path Tracking Control With Delay Compensation for Autonomous Vehicles. *IEEE Trans. Intell. Transp. Syst.* **2021**, *22*, 2979–2989. [CrossRef]
11. Xie, J.; Xu, X.; Wang, F.; Tang, Z.; Chen, L. Coordinated control based path following of distributed drive autonomous electric vehicles with yaw-moment control. *Control Eng. Pract.* **2021**, *106*, 104659. [CrossRef]
12. Wang, Z.; Chen, L.; Cai, Y.; Sun, X.; Wang, H. Adaptive coordinated control strategy for autonomous vehicles based on four-wheel steering. *Proc. Inst. Mech. Eng. Part D J. Automob. Eng.* **2023**, *2023*, 09544070231213755. [CrossRef]
13. Zhang, Y.; Liu, K.; Gao, F.; Zhao, F. Research on Path Planning and Path Tracking Control of Autonomous Vehicles Based on Improved APF and SMC. *Sensors* **2023**, *23*, 7918. [CrossRef]
14. Huang, W.; Ji, X.; Wang, A.; Wang, Y.; Wei, X. Straight-Line Path Tracking Control of Agricultural Tractor-Trailer Based on Fuzzy Sliding Mode Control. *Appl. Sci.* **2023**, *13*, 872. [CrossRef]
15. Shet, R.M.; Lakhekar, G.V.; Iyer, N.C. Intelligent fractional-order sliding mode control based maneuvering of an autonomous vehicle. *J. Ambient Intell. Humaniz. Comput.* **2024**, *15*, 2807–2826. [CrossRef]
16. Wu, L.; Liu, J.; Vazquez, S.; Mazumder, S.K. Sliding Mode Control in Power Converters and Drives: A Review. *IEEE/CAA J. Autom. Sin.* **2022**, *9*, 392–406. [CrossRef]
17. Kebbati, Y.; Ait-Oufroukh, N.; Ichalal, D.; Vigneron, V. Lateral control for autonomous wheeled vehicles: A technical review. *Asian J. Control* **2023**, *25*, 2539–2563. [CrossRef]
18. Zhang, M.; Lin, X.; Ding, Y.; Yin, W.; Qian, Y. Design of path following controllers based on performance index for agricultural vehicle. *Trans. Chin. Soc. Agric. Eng. (Trans. CSAE)* **2012**, *28*, 40–46.
19. Somefun, O.; Akingbade, K.; Dahunsi, F. The dilemma of PID tuning. *Annu. Rev. Control* **2021**, *52*, 65–74. [CrossRef]
20. Liu, W.; Wang, R.; Xie, C.; Ye, Q. Investigation on adaptive preview distance path tracking control with directional error compensation. *Proc. Inst. Mech. Eng. Part I J. Syst. Control Eng.* **2020**, *234*, 484–500. [CrossRef]
21. An, G.; Zhong, Z.; Yang, S.; Yang, L.; Jin, C.; Du, J.; Yin, X. EASS: An automatic steering system for agricultural wheeled vehicles using fuzzy control. *Comput. Electron. Agric.* **2024**, *217*, 108544. [CrossRef]
22. Lee, K.; Choi, H.; Kim, J. Development of Path Generation and Algorithm for Autonomous Combine Harvester Using Dual GPS Antenna. *Sensors* **2023**, *23*, 4944. [CrossRef] [PubMed]
23. Fargnoli, M.; Vita, L.B.; Gattamelata, D.; Laurendi, V.; Tronci, M. A Reverse Engineering Approach to Enhance Machinery Design for Safety. In Proceedings of the DS 70: Proceedings of DESIGN 2012, the 12th International Design Conference, Dubrovnik, Croatia, 21–24 May 2012; Volume 627, pp. 627–636.
24. Yang, Y.; Li, Y.; Wen, X.; Zhang, G.; Ma, Q.; Cheng, S.; Qi, J.; Xu, L.; Chen, L. An optimal goal point determination algorithm for automatic navigation of agricultural machinery: Improving the tracking accuracy of the Pure Pursuit algorithm. *Comput. Electron. Agric.* **2022**, *194*, 106760. [CrossRef]
25. Hu, C.; Ru, Y.; Li, X.; Fang, S.; Zhou, H.; Yan, X.; Liu, M.; Xie, R. Path tracking control for brake-steering tracked vehicles based on an improved pure pursuit algorithm. *Biosyst. Eng.* **2024**, *242*, 1–15. [CrossRef]
26. Zhang, C.; Dong, W.; Xiong, Z.; Hu, Z.; Wang, D.; Ding, Y. Design and Experiment of Fuzzy Adaptive Pure Pursuit Control of Crawler-type Rape Seeder. *Trans. Chin. Soc. Agric. Eng. (Trans. CSAE)* **2021**, *52*, 105–114.